

OPTICAL AND INFRARED PHOTOMETRY OF THE NEARBY SN 2017CBV

JERRICK WEE,¹ NILOTPAL CHAKRABORTY,¹ JIAYUN WANG,¹ AND BRYAN PENPRASE²

¹*Yale-NUS College, 16 College Avenue West, Singapore 138527, Singapore*

²*Soka University of America, 1 University Drive, Aliso Viejo, CA 92656, USA*

(Accepted June 15, 2018)

Submitted to ApJ

ABSTRACT

On 2017 March 11, the DLT40 Transient Discovery Survey discovered SN 2017cbv in NGC5643, a Type 2 Seyfert Galaxy in the Lupus Constellation. SN 2017cbv went on to become a bright Type Ia supernova, with a V_{max} of 11.51 ± 0.05 mag. We present early time optical and infrared photometry of SN 2017cbv covering the rise and fall of over 68 days. We find that SN 2017cbv has a broad light curve $\Delta m_{15}(B) = 0.88 \pm 0.07$, a B -band maximum at 2457840.97 ± 0.43 , a negligible host galaxy reddening where $E(B - V)_{host} \approx 0$, and a distance modulus of 30.49 ± 0.32 to the SN, corresponding to a distance of $12.58^{+1.98}_{-1.71}$ Mpc. We also present the results of two different numerical models we used for analysis in this paper: SALT2, an empirical model for Type Ia supernova optical light curves that accounts for variability components; and SNooPy, the CSP-II light-curve model that covers both optical and near-infrared wavelengths and is used for distance estimates.

Keywords: supernovae: individual (SN 2017cbv) — galaxies: distances and redshifts — dust, extinction — techniques: photometric

1. INTRODUCTION

Type Ia supernovae (SNe) are hypothesized to be the consequence of a thermonuclear explosion of a carbon-oxygen white dwarf (WD) (Nomoto 1982; Nomoto et al. 1984; Woosley & Weaver 1986; Hillebrandt & Niemeyer 2000; Podsiadlowski et al. 2008) or a merger of a pair of white dwarfs in a close binary system (Webbink 1984; Iben & Tutukov 1984). In the former model, the WD accretes material from a non-degenerate secondary companion till it reaches close to the Chandrasekhar mass limit, after which carbon ignites, resulting in the explosion. Different models of this nature can be differentiated on the basis of the secondary companion. The white dwarf can accrete in the following ways: one, from a wind, the “symbiotic channel” (Munari & Renzini 1992); two, by mass transfer from a helium star, also known as the “helium star channel” (Nomoto 1982; Liu et al. 2010; Yoon & Langer 2003) or three, by the Roche-lobe Overflow, the “RLOF channel” (van den Heuvel et al. 1992). The merger of a double-degenerate pair is caused by either the shrinkage of their orbit due to gravitational radiation (Iben & Tutukov 1984; Webbink 1984) or perturbations from additional celestial bodies close to the binary system (Shappee & Thompson 2013; Pejcha, et al. 2013; Antognini, et al. 2014).

SNe Ia are important objects in astronomy and cosmology as they serve as “standard candles” (Riess et al. 1998; Perlmutter & Riess 1999), which help us calculate vast astronomical distances. SNe Ia produce regular patterns in their light curves over the course of a few months, and these patterns have allowed SNe Ia researchers to determine the peak luminosity, host galaxy extinction, and correspondingly, the distances to these objects. The peak luminosity of SNe Ia can be determined by various methods, most notably through variations of the Philips relation (Hamuy et al. 1996; Phillips et al. 1999; Germany et al. 2004; Prieto et al. 2006) and the multicolor light-curve shape (MLCS) method (Riess et al. 1996, 1998; Jha et al. 2007).

The color curves of SNe Ia are important in determining host galaxy extinction. While SNe Ia differ in the shape of their light curves $\Delta m_{15}(B) = 0.75$ to 1.94 (Krisciunas et al. 2003), the color curves of all SNe Ia are thought to evolve in the same way 35 days after $T(B_{max})$, an epoch known as the Lira law regime (Lira 1995). The use of $B - V$ color curves is helpful in determining extinction as the color excess $E(B - V)$ of the SNe Ia can be derived with the data of Galactic dust reddening from the dust maps from Schlegel et al. (1998) and Schlafly & Finkbeiner (2011). However, extinction calculations with optical colors where $A_V = R_V \times E(B - V)$ translate to huge uncertainties

in A_V if $B - V$ has a substantial uncertainty. Extinction calculations would improve if both optical and near-infrared photometry are used (Krisciunas et al. 2007).

The use of both optical and near-infrared (near-IR) photometry of SNe Ia has shown to be crucial in determining extinction in the line of sight of a Type Ia supernova (Wood-Vasey et al. 2008; Mandel et al. 2009; Elias et al. 1985). Particularly, the $V - K$ colors is especially useful for determining extinction as it is the most uniform of all color curves of SNe Ia (Elias et al. 1985).

With data on both the peak luminosity and extinction of a Type Ia supernova, we can derive distance modulus. The distance derived using the Type Ia supernova can also be used to cross-check with other cosmological standard candles in the galaxy, such as the TRGB method and Cepheid variables, which allows us to obtain a precise distance to the galaxy. While there are a lot of data on high- z SNe ($z > 0.01$), data on low- z SNe remain scarce, which introduces substantial errors to the precision of the Hubble constant in the local SNe (Jang et al. 2017). Data of low- z SNe’s distances are critical in constraining the Hubble flow, and hence important to constrain the rate of expansion of the universe.

In this paper, we present early time optical and infrared photometry of the low- z SN 2017cbv. SN 2017cbv (SN) was discovered by S. Valenti et al.¹ on 2017 March 10 UT (= Julian Date 2,457,822.671), at right ascension $14^{\text{h}}32^{\text{m}}34^{\text{s}}.420$ and declination of $-44^{\circ}08'02''738$. The host galaxy of the SN is a Type 2 Seyfert galaxy NGC5643. The galaxy has a redshift of 0.003999 and its heliocentric velocity is 1199 km s^{-1} (Koribalski et al. 2004). Coincidentally, NGC5643 was also the host to another supernova, SN 2013aa, discovered in 2013 (Sternberg et al. 2014). Spectroscopic data of SN 2017cbv by Hosseinzadeh et al.² from the Las Cumbres Observatory determined SN 2017cbv to be a Type Ia supernova two weeks before maximum light.

2. OBSERVATIONS

We used the Yale SMARTS 1.3m Telescope at the Cerro Tololo Inter-American Observatory (CTIO) for optical and near-infrared (near-IR) observation in $BVRIZJHK$ bandpasses. The images were taken with the ANDICAM instrument, an imager permanently mounted on the 1.3m telescope that takes simultaneous optical and infrared data. The ANDICAM instrument uses the standard Johnson BV filters, Kron-Cousins R

¹ <https://wis-tns.weizmann.ac.il/object/2017cbv/discovery-cert>

² <https://wis-tns.weizmann.ac.il/object/2017cbv/classification-cert>

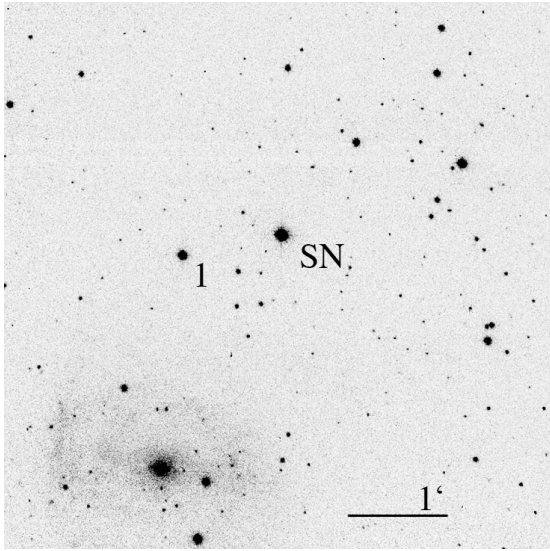


Figure 1. V-band image of SN 2017cbv off NGC 5643 obtained with the CTIO 1.3m telescope on 2017 March 27. The exposure time was 15s. The local photometric standard is numbered. The bar corresponds to $1'$. North is up, and east to the left. The supernova is marked 'SN', in the center of the image.

and I filters, standard CIT/CTIO JHK filters, and a $1.05\mu\text{m}$ Y filter. The optical field of view is $6.3' \times 6.3'$, while the IR field of view is $2.34' \times 2.34'$. With the CCD readout in 2×2 binning mode, the ANDICAM instrument gives a plate scale on the 1.3m telescope of $0.369'' \text{ pixel}^{-1}$ for optical imaging and $0.274'' \text{ pixel}^{-1}$ for near-IR imaging. Further information can be found on the ANDICAM instrument specification website³.

We started taking optical images of the SN on 2017 March 14, and started taking infrared images on 2017 March 18. Our observations ended on 2017 June 9, for a total of 68 nights of data. Figure 1 is a V-band optical image in which we identify the location of the SN and the local field standard, with Table 1 presenting the optical photometric sequence of the local field standard. Figure 2 is a J-band near-IR image which shows the location of the SN and the field standards. The data on the local field standards for the near-IR can be found on Table 2.

We conducted the photometric reduction of the optical data using the Photutils's aperture photometry tool (Bradley et al. 2016), a part of the Python-based package Astropy (Astropy Collaboration et al. 2013). The use of aperture photometry over point spread function (PSF) fitting is justified on the account that the SN is a low- z supernova and that the SN appears at a substantial angular distance ($2.57'$) from its host galaxy.

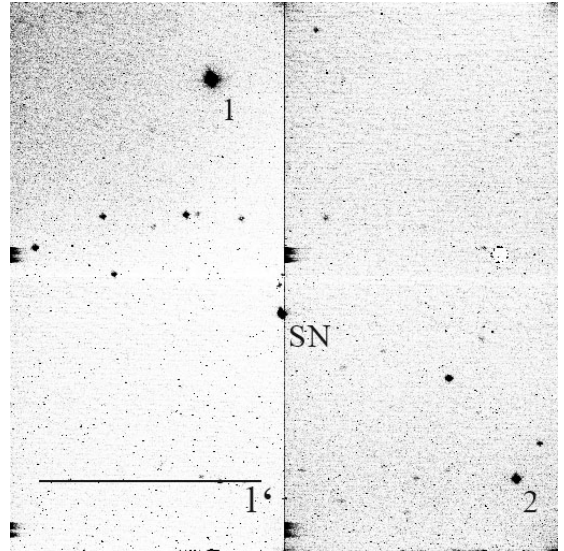


Figure 2. J-band image of SN 2017cbv off NGC 5643 obtained with the CTIO 1.3m telescope on 2017 March 27. The exposure time was 15s. The local photometric standards are numbered. The bar corresponds to $1'$. The supernova is marked 'SN', in the center of the image. North is right, east is down.

This angular separation from the host galaxy reduces the chance that SN would be contaminated by the other sources of photons in the aperture radii.

We estimated the magnitudes for a set of reference stars in the field of view of the SN using the mean value of five nights of observations. Our photometry for individual nights was computed using the grid of reference stars in the field, and these differentiated magnitudes were converted to $BVRI$ magnitudes using zero points derived from observations of photometric standards, described in Section 2.1.

While there appears to be multiple bright stars in the field of view for the optical images, we have two problems with using multiple reference stars. One, our field of view is not consistent as we changed our coordinates throughout our observation. That severely limits our available reference stars to a small field of view centered on the galaxy. Two, depending on the exposure for a particular night, the reference stars available have a signal-to-noise ratio that is 5 to 8 times lower than the SN and Star 1, which reduces the quality of our light curves and increases errors in our results. For these reasons, we did not use more reference stars for our optical photometry than the ones labeled.

The near-IR data are reduced using the astronomy software Cyanogen Imaging MaxIm DL's photometric tool, which has the in-built capability to identify, track, and photometer objects across images using aperture photometry. We used Star 2 (Figure 2) for YJH filter

³ <http://www.astronomy.ohio-state.edu/ANDICAM/detectors.html>

magnitudes and Star 1 (Figure 2) for K filter magnitudes for our differential photometry. We present the $BVR IYJHK$ light curves in Figure 3.

We performed a Lomb-Scargle periodicity analysis on both reference stars with 152 and 149 photometric V -band data points for Star 1 and Star 2 respectively over 1798 days from the Catalina Sky Survey (Drake, et al. 2009). Both stars have significant false alarm probabilities that makes them highly unlikely to be variables. We also conducted a χ^2 fit test with a non-varying model for both reference stars and found that the χ^2 fit was consistent with a model of non-variability. Both reference stars have been extensively observed by the Catalina Sky Survey and were not determined to be variables (Drake, et al. 2017). The combination of our tests and the lack of variability found for both of our reference stars from Drake, et al. (2017) gives us good confidence that the two reference stars are not variables.

Both random errors from our sky and background subtraction and systematic errors in zero points were computed in our systematic error budget.

2.1. Zero Points

We carried out standard calibrations for the optical zero points using the Landolt standards, namely: Ru149, Ru149A, Ru194B, and Ru194C (Landolt 1992). Optical observations of the Landolt standard field were made with the same telescope and camera at CTIO over 5 nights between 2017 March 24 and 2017 April 21. The calibrations involved analyzing the intensities of the 4 standards stars each night alongside the airmass for calculating extinction.

From the dataset of each standard star, we arrived at an average zero point and its standard deviation. The zero points of the $BVRI$ bands were calibrated with extinction and color term corrections, given in Equation (1). In Table 3, we present the extinction and color term coefficients we used for our calibrations and the error of the data involved.

$$ZP_i = m_{inst_i} - M - E_i(X-1) - C_i(m_{inst_a} - m_{inst_b}) \quad (1)$$

where ZP_i is the zero point of a filter i , m_{inst_i} is the instrumental magnitude for a given filter i , M is the literature magnitude, E_i is the extinction coefficient for a given filter i , $C_i(m_{inst_a} - m_{inst_b})$ is the color term coefficient for a given filter i .

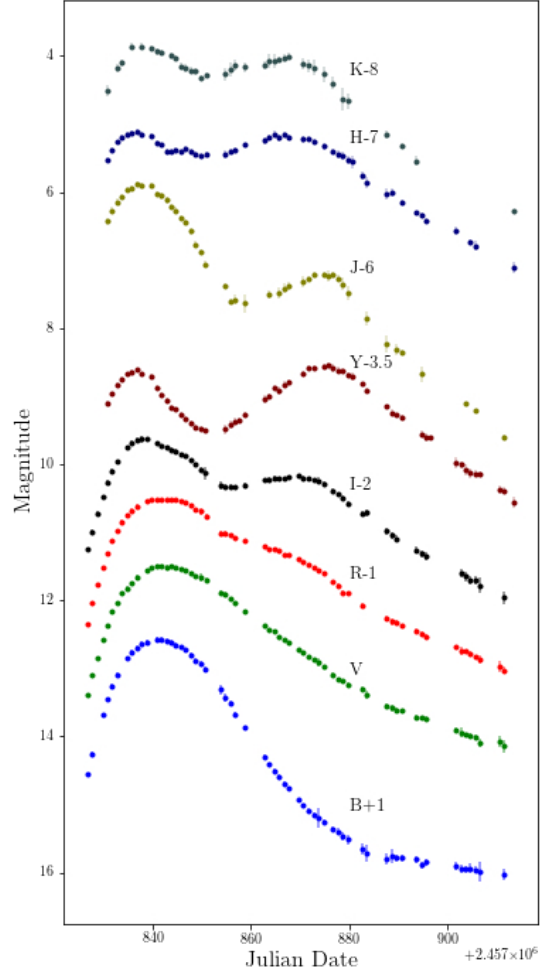


Figure 3. Light curves of SN 2017cbv in the optical and near-infrared, with respective offset.

We obtained the extinction⁴ and color term⁵ coefficients from the CTIO's calibration pages. The final zero points and the error used are the mean values of the zero points and standard deviations calculated from the independent observations of the different standard stars.

The zero points of the $YJHK$ bands were calibrated using the Persson standard system (Persson et al. 1998) with the P9144 field. The calibration involved independent observations of reference stars taken during 7 nights between 2017 March 21 and 2017 June 9. The Y magnitudes for the P9144 field in the Persson standard system are obtained from Krisciunas et al. (2017). The procedure for data analysis and aperture choice of the near-IR

⁴ <http://www.ctio.noao.edu/noao/content/13-m-smarts-photometric-calibrations-bvri>

⁵ <http://www.ctio.noao.edu/noao/content/photometric-zero-points-color-terms>

Table 1. Optical Photometry Sequence Near SN 2017cbv

Star ID	α (J2000)	δ (J2000)	V	$B - V$	$V - R$	$V - I$
SN	14 ^h 32 ^m 34 ^s .420	−44°08′02.738″
1	14 ^h 32 ^m 39 ^s .982	−44°08′17.340″	12.806 (045)	1.206 (113)	0.7276 (085)	1.364 (103)

Table 2. Infrared Photometry Sequence Near SN 2017cbv

Star ID	Y	J	H	K
1	9.564 (064)
2	12.993 (033)	12.706 (045)	12.495 (037)	...

Table 3. Optical Extinction and Color Term Coefficients

Band	Extinction	Color Term
B	0.251	$-0.079(B - V)$
V	0.149	$0.018(B - V)$
R	0.098	$-0.03(V - R)$
I	0.066	$0.045(V - I)$
Y	0.083	-
J	0.010	$-0.034(J - H)$
H	0.055	$0.022(J - H)$
K	0.085	$-0.003(J - K)$

Table 4. Calibrated Zero Points of the $BVRIYJHK$ Bands

Filter	Zero Point	Error
B	22.019	0.054
V	21.758	0.030
R	21.559	0.022
I	20.939	0.032
Y	18.274	0.022
J	18.177	0.028
H	18.305	0.030
K	17.764	0.037

zero points were the same as those of the optical zero points.

In Table 4, we present the zero points of the $BVRIYJHK$ bands. The complete optical and near-IR photometric cadence is listed in Table 5.

3. RESULTS

To analyze our supernova data, we used two different numerical models to produce fits to our lightcurves: SALT2 (using SNcosmo, [Guy et al. 2007](#)) and SNooPy ([Burns et al. 2011](#)). Each model has its own fit parameters and each model gives separate insights to the supernova and the host galaxy.

3.1. SALT2 Modelling

We fit our optical light curves using SALT2 ([Guy et al. 2007](#)). Using SNcosmo ([Barbary et al. 2016](#)) we extracted values for the different fit parameters (x_0, x_1 and c) in the SALT2 model, where the flux of the source is given as

$$F(SN, p, \lambda) = x_0 \times [M_0(p, \lambda) + x_1 M_1(p, \lambda) + \dots] \times \exp[cCL(\lambda)] \quad (2)$$

where p is the rest-frame time since the date of maximum luminosity in B -band (the phase), and λ the wavelength in the rest-frame of the SN. $M_0(p, \lambda)$ is the average spectral sequence whereas $M_k(p, \lambda)$, for $k > 0$, are additional components that describe the variability of SNe Ia light curve. $CL(\lambda)$ represents the average color correction law. In the models from SALT2, the optical

Table 5. Optical and Near-IR Photometric Cadence of SN 2017cbv

Julian Date (2457000)	Exposure Time (V)	<i>B</i>	<i>V</i>	<i>R</i>	<i>I</i>	<i>Y</i>	<i>J</i>	<i>H</i>	<i>K</i>
826.759	15	13.557(064)	13.398(041)	13.352(033)	13.255(054)
827.742	15	13.253(067)	13.103(041)	13.038(032)	12.997(057)
828.782	30	12.844(042)	12.776(035)	12.725(057)
829.781	30	12.685(067)	12.572(046)	12.518(033)	12.483(054)
830.763	30	12.462(069)	12.366(044)	12.311(034)	12.266(054)	12.598(035)	12.433(046)	12.531(032)	12.518(083)
831.773	30	12.263(063)	12.172(048)	12.128(049)	12.102(065)	12.470(030)	12.277(049)	12.380(037)
832.755	30	12.095(065)	12.035(045)	11.985(038)	11.961(063)	12.339(038)	12.153(051)	12.269(037)	12.176(064)
833.730	15	11.902(052)	11.845(047)	12.247(032)	12.076(040)	12.201(038)	12.102(048)
834.677	15	11.857(069)	11.824(056)	11.758(051)	11.762(079)	12.175(033)	11.965(041)	12.153(044)
835.783	15	11.766(079)	11.749(057)	11.681(053)	11.695(079)	12.144(034)	11.947(045)	12.139(039)	11.860(052)
836.759	15	11.707(087)	11.658(058)	11.616(053)	11.650(085)	12.117(031)	11.885(039)	12.116(041)
837.747	15	11.640(088)	11.636(086)	12.178(031)	11.905(042)	12.152(043)	11.862(051)
838.802	15	11.616(088)	11.563(054)	11.539(048)	11.635(074)
839.772	15	11.512(047)	11.530(039)	12.204(031)	11.906(038)	12.175(037)	11.884(045)
840.768	15	11.575(085)	11.509(047)	11.516(039)	11.698(060)	12.373(033)	12.024(044)	12.272(035)	11.940(044)
841.807	15	11.586(077)	11.508(048)	11.516(044)	11.730(059)	12.477(035)	12.061(046)	12.313(038)	11.958(045)
842.789	15	11.594(076)	11.511(047)	11.522(039)	11.757(060)	12.562(036)	12.121(048)	12.406(037)
843.791	15	11.614(082)	11.505(047)	11.512(038)	11.791(059)	12.661(030)	12.222(044)	12.398(034)	11.999(047)
844.733	15	11.664(073)	11.521(046)	11.516(038)	11.811(058)	12.697(032)	12.274(047)	12.392(038)	12.031(046)
845.756	15	11.691(074)	11.540(048)	11.541(039)	11.862(057)	12.765(034)	12.384(043)	12.400(042)	12.155(048)
846.665	15	11.733(075)	11.555(048)	11.561(039)	11.883(058)	12.833(033)	12.443(044)	12.361(039)	12.178(064)
847.755	15	11.806(078)	11.609(049)	11.612(040)	11.949(057)	12.895(033)	12.582(043)	12.408(044)	12.216(057)
848.757	15	11.891(079)	11.637(049)	11.659(040)	12.007(058)	12.965(037)	12.773(052)	12.445(040)	12.229(050)
849.735	15	11.940(081)	11.662(116)	11.698(118)	12.080(058)	12.976(030)	12.873(039)	12.464(040)	12.328(046)
850.793	15	12.017(082)	11.703(094)	11.771(093)	12.135(179)	13.009(034)	13.063(045)	12.449(037)	12.283(047)
853.722	15	12.314(142)	11.892(073)	12.010(071)	12.312(115)
854.764	30	12.428(119)	11.913(064)	12.016(058)	12.334(098)	12.989(078)	13.382(035)	12.452(068)	12.272(092)
855.769	30	12.513(084)	11.978(056)	12.041(050)	12.339(080)	12.924(062)	13.605(045)	12.407(048)	12.202(101)
856.744	30	12.672(076)	12.045(050)	12.080(043)	12.342(070)	12.875(054)	13.584(067)	12.377(041)	12.143(088)
857.649	30	12.850(025)
858.776	30	12.873(070)	12.160(046)	12.122(039)	12.311(062)	12.765(041)	13.638(140)	12.309(032)	12.161(073)
862.723	30	13.303(066)	12.371(048)	12.209(039)	12.229(058)	12.543(056)	12.244(052)	12.137(059)
863.749	30	13.409(060)	12.442(043)	12.240(038)	12.221(048)	12.506(038)	13.505(056)	12.207(040)	12.069(102)
864.795	30	13.510(067)	12.458(042)	12.241(034)	12.202(061)	12.388(042)	12.149(045)	12.078(100)
865.754	30	13.594(066)	12.530(040)	12.269(033)	12.212(051)	12.422(061)	13.484(087)	12.206(047)	12.053(045)
866.748	30	13.695(067)	12.580(040)	12.322(037)	12.207(049)	12.328(045)	13.414(078)	12.163(041)	12.039(061)
867.664	30	13.771(063)	12.612(044)	12.330(042)	12.197(050)	12.297(042)	13.379(066)	12.202(037)	12.008(048)
869.736	30	13.935(065)	12.723(044)	12.394(034)	12.177(049)
870.657	30	14.012(060)	12.775(041)	12.438(034)	12.202(051)	12.161(041)	13.318(080)	12.226(049)	12.123(088)
871.726	30	14.087(065)	12.826(041)	12.481(034)	12.215(053)	12.094(038)	13.278(036)	12.219(049)	12.147(099)
872.717	30	14.148(068)	12.870(042)	12.517(034)	12.233(052)	12.090(041)	13.220(046)	12.258(039)	12.177(115)
873.732	30	14.201(291)	12.915(121)	12.562(042)	12.244(112)
874.716	30	14.268(084)	12.971(051)	12.605(043)	12.291(061)	12.070(034)	13.208(035)	12.332(047)	12.269(119)
875.624	30	12.038(029)	13.239(078)
876.648	30	14.369(085)	13.089(052)	12.731(048)	12.389(062)	12.088(053)	13.214(048)	12.408(038)	12.399(102)
877.591	30	14.401(103)	13.160(057)	12.779(053)	12.444(066)	12.123(053)	13.270(053)	12.448(054)
878.630	30	14.462(125)	13.186(064)	12.887(058)	12.498(071)	12.128(044)	13.351(087)	12.474(059)	12.644(170)
879.612	30	14.515(139)	13.235(069)	12.898(062)	12.582(074)	12.184(040)	13.484(097)	12.531(054)	12.669(120)
880.574	30	12.212(053)	12.563(089)
882.563	30	14.649(175)	13.311(076)	13.081(093)	12.729(089)	12.318(025)	12.759(069)
883.596	30	14.709(258)	13.392(109)	12.709(106)	12.419(045)	13.862(110)	12.861(080)
887.609	30	14.797(171)	13.552(088)	13.271(077)	12.984(101)	12.659(033)	14.227(127)	13.029(085)	13.152(066)
888.593	30	14.761(218)	13.584(101)	13.319(085)	13.050(104)	12.747(052)	13.019(062)
889.585	30	14.784(102)	13.618(065)	13.326(063)	13.098(098)	12.783(032)	14.317(091)
890.602	30	14.790(104)	13.629(063)	13.381(059)	12.814(047)	14.362(035)	13.151(046)	13.319(038)
893.627	30	14.811(114)	13.714(070)	13.450(066)	13.262(100)	13.309(032)	13.549(074)
894.603	30	14.886(105)	13.727(067)	13.498(068)	13.321(108)	13.057(044)	14.678(119)	13.338(032)
895.580	30	14.853(122)	13.744(070)	13.531(074)	13.351(121)	13.108(066)	13.425(032)
896.560	30	13.113(025)
901.563	30	14.913(129)	13.913(078)	13.691(075)	13.476(088)	13.569(068)
902.645	90	14.944(116)	13.947(149)	13.746(128)	13.608(121)	13.507(054)
903.720	90	14.949(108)	13.980(070)	13.750(071)	13.654(136)	13.587(087)	15.116(035)
904.582	90	14.943(142)	13.983(083)	13.788(080)	13.699(126)	13.634(073)	13.733(045)
905.556	90	14.960(108)	14.006(071)	13.836(074)	13.700(127)	13.638(048)	15.222(035)	13.791(067)
906.539	90	14.981(299)	14.095(140)	13.867(138)	13.781(221)	13.638(031)
910.542	90	14.070(162)	13.976(158)	13.876(054)
911.551	90	15.025(177)	14.142(186)	14.028(117)	13.958(189)	13.889(053)	15.598(035)
913.546	90	14.060(082)	14.103(083)	14.290(038)

NOTE—Julian dates refer to the median Julian dates for all the images taken in a night. Exposure times represented in the table is for *BVRJHK* bandpasses. The exposure time for *I* and *Y* filter is two times longer than the exposure times listed on the table for the respective Julian dates.

depth is expressed using a color offset with respect to the average at the date of maximum luminosity in B -band, $c = (B - V)_{max} - (B - V)$. This parametrization models the part of the color variation that is independent of phase, whereas the remaining color variation with phase is accounted for by the linear components. In Equation (2), x_0 is the normalization of the spectral energy distribution sequence, and x_k for $k > 0$, are the intrinsic parameters of the SN (such as a stretch factor). To summarize, while (M_k) and CL are properties of the global model, (x_k) and c are parameters of a given supernova and hence differ from one SN to another.

To perform accurate fits to observational data from the CTIO telescope, we registered the CTIO filters⁶ into the Sncosmo system, which uses *SDSS* filters for its default bandpass. After registering the CTIO *BVRI* filter band passes in the Sncosmo system, we were able to input our observed photometric magnitudes into the program to enable the modelling of the flux for the SN.

Out of the 5 free parameters (z, t_0, x_0, x_1, c) for the Sncosmo program we set the redshift to $z \approx 0.004$ for our SN based on previous observations in the literature (Koribalski et al. 2004). The fit is represented in Figure 4. The light curve models derived the time for maximum brightness where $t_0 = 2457840.782 \pm 0.017$, corresponding to 2017 March 28, 06:46:04.8 UT.

3.2. SNooPy Modelling

We used the CSPII light-curve fitting code Supernovae in Object Oriented Python (SNooPy, Burns et al. 2011) to fit the light curve of SN 2017cbv in the optical and infrared. SNooPy has the prime benefit of modelling SNe Ia in a wide range of wavelengths, as it simultaneously fits SNe Ia light curves in both the optical and near-IR. SNooPy also has a *systematics* function, where it calculates the date of B -band peak $T_{max}(B)$, color excess of host galaxy $E(B - V)_{host}$, the change of B -band magnitude from maximum to 15 days after maximum $\Delta m_{15}(B)$, and the distance modulus.

The model that we used in SNooPy is the EBV_{model} . The light curve model is a variation of the model given by Prieto et al. (2006):

$$m_X(t - t_{max}) = T_Y((t' - t_{max})/(1+z), \Delta m_{15}) + M_Y(\Delta m_{15}) \\ + \mu + R_X E(B - V)_{gal} + R_Y E(B - V)_{host} + \\ K_{X,Y}(z, (t' - t_{max})/(1+z), E(B - V)_{host}, E(B - V)_{gal})$$

where m_X is the observed magnitude in band X , t_{max} is the time of B maximum, Δm_{15} is the decline rate pa-

rameter (Phillips 1993), M_Y is the absolute magnitude in filter Y in the rest-frame of supernova, $E(B - V)_{gal}$ and $E(B - V)_{host}$ are reddening due to galactic foreground and host galaxy, respectively, R_X and R_Y are the total-to-selective absorptions for filters X and Y , respectively, K_{XY} is the cross-band K -correction from rest-frame X to observed filter Y . SNooPy uses the Schlegel maps for the handling of galactic extinction (Burns et al. 2011).

For the fit, we registered the CTIO *BVRJHK* filters to SNooPy which uses CSPII filters as its default bandpass. As there was no transmission data for ANDICAM Y bandpass, we used the CSPII Y filter for the fit for our Y bandpass. The resulting fit with SNooPy presented in Figure 5.

With CTIO's filter transmission data and our *BVRJHK* light curves, SNooPy's *systematics* function yields the following results. $T_{max}(B)$ is on 2017 March 28, 11:09:36.0 UT (JD = 2457840.965 \pm 0.088 with systematic model error of 0.340). The color excess of host galaxy is determined to be -0.090 ± 0.009 with a systematic model error of ± 0.060 . The Δm_{15} is 0.877 ± 0.010 with a systematic model error of ± 0.060 . The distance modulus is 30.499 ± 0.008 with a systematic model error of ± 0.309 .

4. DISCUSSION

4.1. Optical Light Curves

A typical Type Ia supernova has a B -band decline rate $\Delta m_{15}(B) = 1.1$ mag (Phillips et al. 1999), and this parameter varies roughly from 0.75 to 1.94 (Krisciunas et al. 2003). Compared to the $\Delta m_{15}(B)$ variation, SN 2017cbv has a broad decline of $\Delta m_{15}(B) = 0.877 \pm 0.070$ mag (including systematic model error) according to the SNooPy model.

As expected of optical light curves of SNe Ia, the B -band decline rate of the SN is the most rapid, followed by V -band, R -band, and I -band respectively. We also see the expected secondary bump in the I optical band and a shoulder in the R band at JD \approx 2457869.70.

The relatively faster B -band decline rate for SNe Ia is caused by the increasing absorption by Fe II and Co II lines as the ejecta cools, which blocks transmissivity of bluer wavelength bands and simultaneously improve transparency at a longer wavelength post maximum light of SNe Ia (Kasen 2006).

4.2. Near-Infrared Light Curves

Our near-IR *YJHK* light curves shows the expected secondary maximum for near-IR wavelengths. The secondary maximum is noteworthy for the Y and H bands, where the secondary peaks are brighter than the pri-

⁶ <http://www.astronomy.ohio-state.edu/ANDICAM/detectors.html>

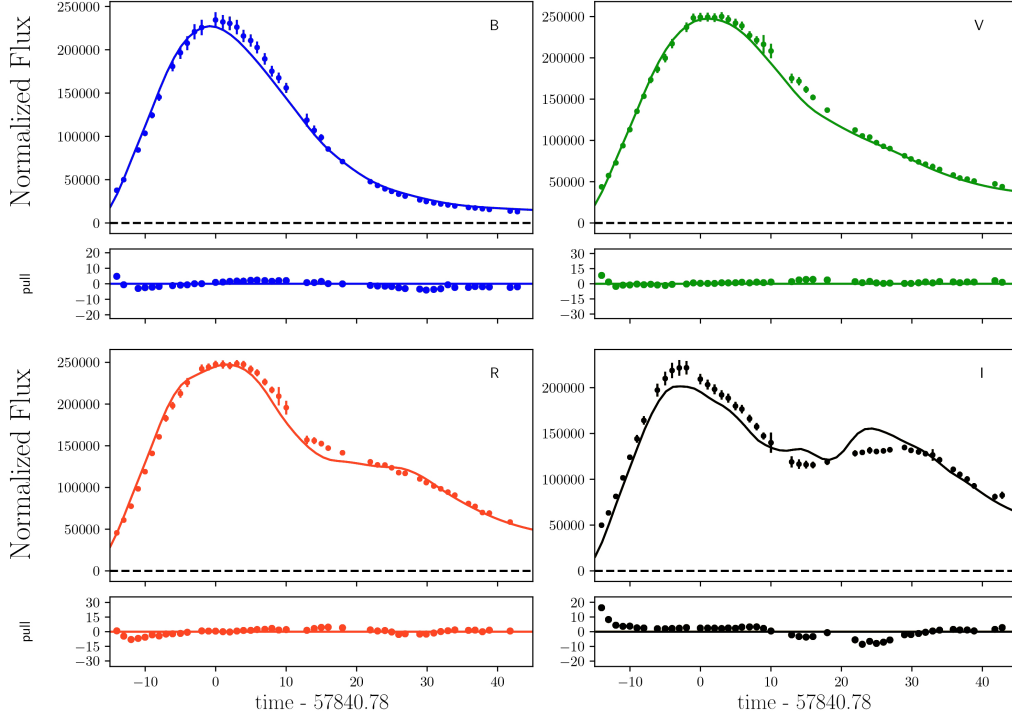


Figure 4. Fits to the SN's *BVRI* light curves using SNcosmo.

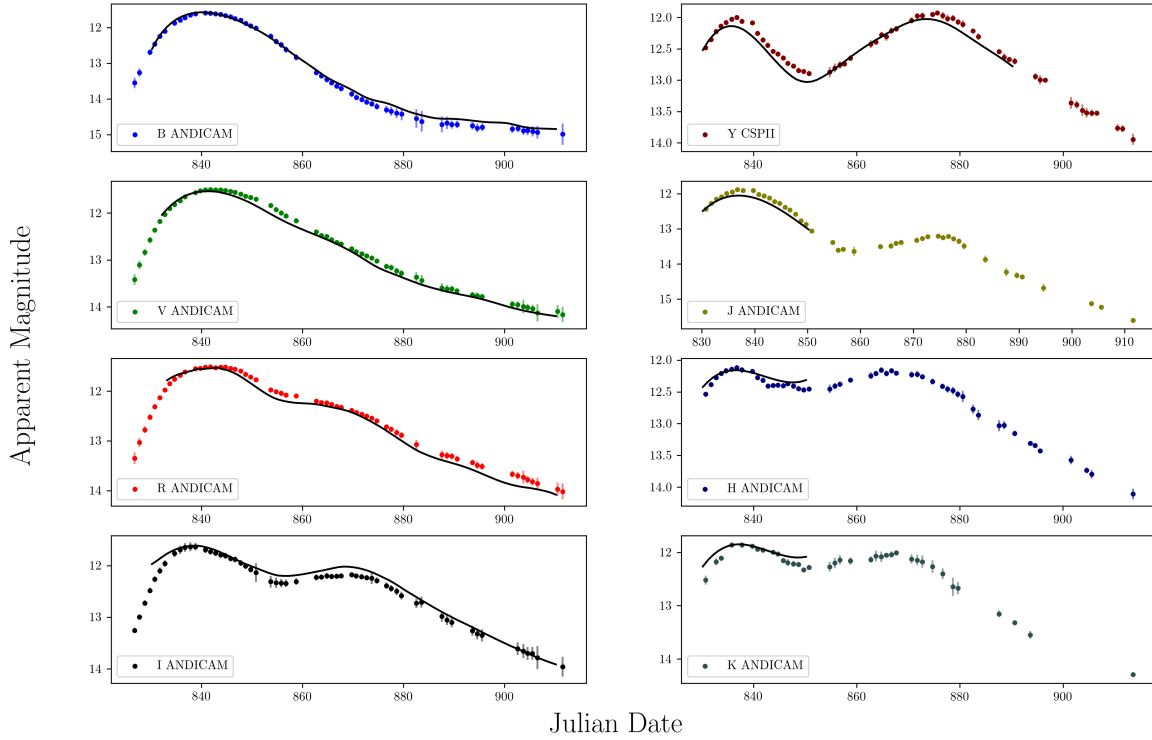


Figure 5. SNOoPy fits for the SN using CTIO's ANDICAM *BVRIJHK* filters and CSPII *Y* filter.

mary peaks, a phenomenon not uncommon in SNe Ia’s near-IR light curves (Phillips et al. 2013).

The mechanics of the secondary maximum in the near-IR is similar to that of the I and R bump in Kasen’s models (Kasen 2006), where the ejecta cools and becomes transparent in the near-IR, allowing photons in the near-IR wavelengths to escape the ejecta. Future work can shed light on the astrophysics of the secondary bump by comparing the shape of the SN’s high cadence light curves with other SNe Ia.

4.3. Reddening and Extinction

From 30 to 90 days after V -band maximum, the color evolution for unreddened $B - V$ colors of SNe Ia is thought to be uniform (Lira 1995) in what is called the Lira law regime. The spectra of the SN during Lira law regime is uniform throughout the late epoch as the Fe-Ni-Co core dominates the spectrum that is rapidly evolving into a supernova phase (Kasen 2006). Knowing the intrinsic $B - V$ colors of a Type Ia supernova allows us to calculate the extinction of the SN, in the form of the ratio of total-to-selective dust absorption, R_V . Figure 6 shows the $B - V$ color curve of SN 2017cbv.

As SNe Ia have varying $B - V$ colors throughout the evolution of their light curves, there are several views as to which part of the $B - V$ curve provides us with the most meaningful $B - V$ value to use for calculating color excess. Jha et al. (2007), through an analysis of a large sample of SNe Ia, found that the intrinsic colors of SNe Ia are identical and well-described by a Gaussian distribution at 35 days post B -band maximum. We take Jha’s intrinsic $B - V$ of 1.054 ± 0.049 mag at t_{35} (Jha et al. 2007). Since our observed $B - V$ at t_{35} is 1.164 ± 0.08 mag, the color excess $E(B - V)$ of the SN at t_{35} is 0.11 ± 0.129 . With the Galactic reddening of 0.145 ± 0.001 in the coordinates of the SN (Schlafly & Finkbeiner 2011), the host galaxy reddening is negligible. The findings are consistent with SNooPy’s *systematics* function, where the function also derived zero host galaxy reddening using the Schlegel maps. Since extinction is negligible ($A_V \approx 0$), it is not possible to determine the total-to-selective ratio R_V of the host galaxy NGC5643.

4.4. Distance

SNooPy’s *systematics* function provides a distance modulus to the SN using the calibrated absolute magnitudes of the SN using Prieto et al.’s method (Prieto et al. 2006) as stated above. Prieto’s method uses the concordance model and assumes $H_0 = 72$ km s $^{-1}$ Mpc $^{-1}$ (Prieto et al. 2006). The averaged distance modulus $(m - M)_{\text{BVRI}}$ of the SN based on SNooPy’s *systematics* function is 30.499 ± 0.008 with a system-

atic model error of ± 0.309 , corresponding to a distance of $12.583^{+1.977}_{-1.709}$ Mpc. The distance modulus is in agreement with the Galactocentric GSR distance of $(m - M) = 30.83 \pm 0.15$ and the average redshift-independent distance $(m - M) = 30.25 \pm 0.44$ to the host galaxy NGC5643. The information on the distances is obtained from the NASA/IPACExtragalactic Database. The redshift-independent distance and the Galactocentric GSR distance for NGC5643 disagree with each other, but interestingly, our results fall within the range of both distances.

5. CONCLUSION

We have presented optical and near-IR photometry of SN 2017cbv. We found that the SN is a broad decliner with a $\Delta m_{15}(B) = 0.877 \pm 0.070$ mag. The SN also exhibit the typical SNe Ia light curves, with the rapid decline of B and V bands, and the slight secondary bump in the R and I in the optical light curves. We also observe the secondary maximums for the Y and H bands that are brighter than their primary maximums, and the characteristic secondary bump in the J and K bands. From the Δm_{15} , we estimated M_V (Prieto et al. 2006; Phillips 1993) and calculated $M_V = -19.380 \pm 0.027$ for the SN. From SALT2, we derived the time of maximum brightness corresponded to be $t_0(B) = 2457840.782 \pm 0.017$, which is in agreement with SNooPy’s figure of $T_{\text{max}}(B) = 2457840.965 \pm 0.088 \pm 0.340$.

With the Schlegel and Schlafly maps, we also find that SN 2017cbv was unreddened by host galaxy dust, where $E(B - V)_{\text{host}} \approx 0$. Since host galaxy extinction is negligible, the total-to-selective ratio R_V cannot be determined. We also derived a distance modulus of the object where $(m - M) = 30.499 \pm 0.008 \pm 0.309$, corresponding to a distance of $12.583^{+1.977}_{-1.709}$ Mpc. The distance of the SN is consistent with both redshift-dependent and redshift-independent derivations of the distance to its host galaxy.

Considering the proximity of the SN, our distance determination to the SN has important implications for cosmologists working on the precision of the Hubble constant. Notably, our distance determination could assist the Carnegie-Chicago Hubble Program (Beaton et al. 2016), which relies on RR Lyrae zero-point, the TRGB method, and local SNe Ia that is not in the Hubble flow where $z < 0.01$. A comparison of the SN’s $B - V$ color curves with CSPH photometric data of ten other low- z SNe Ia (Stritzinger et al. 2011) in Figure 6 shows that the SN conforms to the usual color evolution of other SNe Ia, which makes it ideal for further studies.

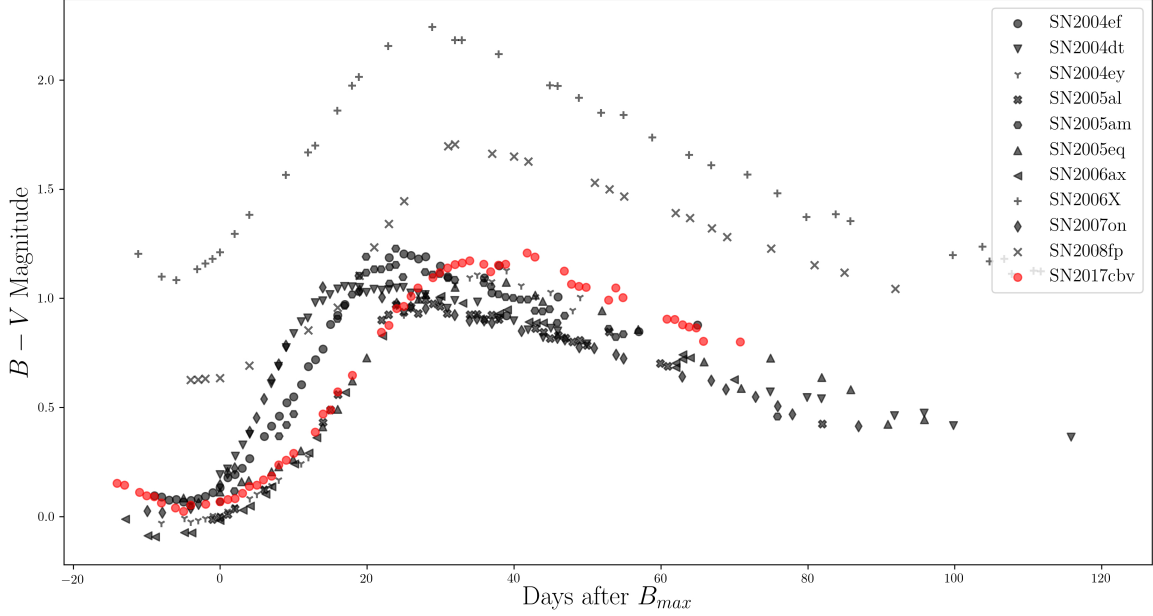


Figure 6. $B - V$ color curve of SN 2017cbv in comparison with photometric data of low- z SNe Ia.

We like to thank Mark Phillips for reading through and providing critical comments for the draft of our paper and Rohan Naidu for his help in developing new Python routines for analysis of the optical photometry of this project. We also like to thank Rachael Beaton and Ben Shappee for discussions on the supernova and Chris Burns for his help with configuring SNOOPy for our supernova modelling.

This work is supported and funded by Yale-NUS College and JY Pillay Foundation. B.E.P. would like to acknowledge the support from Yale-NUS College, and

from funding from NSF grant (AST-1440341) and an NSF PIRE Grant 1545949.

Facilities: CTIO 1.3m, LCRO 0.3m

Software: Astropy (Astropy Collaboration et al. 2013), Cyanogen Imaging MaxIm DL v6 (<http://diffractionlimited.com/product/maxim-dl/>), SNCosmo (Barbary et al. 2016), SNOOPy (Burns et al. 2011)

REFERENCES

- Astropy Collaboration, Robitaille, T. P., Tollerud, E. J., et al. 2013, *A&A*, 558, A33
- Antognini, J. M., Shappee, B. J., Thompson, T. A., et al. 2014, *MNRAS*, 439, 1079.
- Barbary, K., Barclay, T., Biswas, R., et al. 2016, *Astrophysics Source Code Library*, ascl:1611.017
- Beaton, R. L., Freedman, W. L., Madore, B. F., et al. 2016, *ApJ*, 832, 210
- Burns, C. R., Stritzinger, M., Phillips, M. M., et al. 2011, *AJ*, 141, 19
- Bradley, L., Sipocz, B., Robitaille, T., et al. 2016, *Astrophysics Source Code Library*, ascl:1609.011
- Cardelli, J. A., Clayton, G. C., & Mathis, J. S. 1989, *ApJ*, 345, 245
- Drake, A. J., Djorgovski, S. G., Mahabal, A., et al. 2009, *ApJ*, 696, 870.
- Drake, A. J., Djorgovski, S. G., Catelan, M., et al. 2017, *MNRAS*, 469, 3688.
- Elias, J. H., Matthews, K., Neugebauer, G., & Persson, S. E. 1985, *ApJ*, 296, 379
- Germany, L. M., Reiss, D. J., Schmidt, B. P., Stubbs, C. W., & Suntzeff, N. B. 2004, *A&A*, 415, 863
- Guy, J., Astier, P., Baumont, S., et al. 2007, *A&A*, 466, 11
- Gilfanov, M., & Bogdán, Á. 2010, *Nature*, 463, 924
- Hamuy, M., Phillips, M. M., Suntzeff, N. B., et al. 1996, *AJ*, 112, 2391
- Hatt, D., Beaton, R. L., Freedman, W. L., et al. 2017, *ApJ*, 845, 146
- Hillebrandt, W., & Niemeyer, J. C. 2000, *ARA&A*, 38, 191
- Iben, I., Jr., & Tutukov, A. V. 1984, *ApJS*, 54, 335
- Jang, I. S., Hatt, D., Beaton, R. L., et al. 2017, *arXiv:1703.10616*

- Jha, S., Garnavich, P. M., Kirshner, R. P., et al. 1999, *ApJS*, 125, 73
- Jha, S., Riess, A. G., & Kirshner, R. P. 2007, *ApJ*, 659, 122
- Kasen, D. 2006, *ApJ*, 649, 939
- Koribalski, B. S., Staveley-Smith, L., Kilborn, V. A., et al. 2004, *AJ*, 128, 16
- Krisciunas, K., Hastings, N. C., Loomis, K., et al. 2000, *ApJ*, 539, 658
- Krisciunas, K., Suntzeff, N. B., Candia, P., et al. 2003, *AJ*, 125, 166
- Krisciunas, K., Garnavich, P. M., Stanishev, V., et al. 2007, *AJ*, 133, 58
- Krisciunas, K., Contreras, C., Burns, C. R., et al. 2017, *AJ*, 154, 211
- Landolt, A. U. 1992, *AJ*, 104, 340
- Lang, D., Hogg, D. W., Mierle, K., Blanton, M., & Roweis, S. 2010, *AJ*, 139, 1782
- Liu, W.-M., Chen, W.-C., Wang, B., & Han, Z. W. 2010, *A&A*, 523, A3
- Lira, P. 1995, Masters Thesis, Universidad de Chile
- Mandel, K. S., Wood-Vasey, W. M., Friedman, A. S., & Kirshner, R. P. 2009, *ApJ*, 704, 629
- Moll, R., Raskin, C., Kasen, D., & Woosley, S. E. 2014, *ApJ*, 785, 105
- Munari, U., & Renzini, A. 1992, *ApJL*, 397, L87
- Nomoto, K. 1982, *ApJ*, 253, 798
- Nomoto, K., Thielemann, F.-K., & Yokoi, K. 1984, *ApJ*, 286, 644
- Pejcha, O., Antognini, J. M., Shappee, B. J., et al. 2013, *MNRAS*, 435, 943.
- Persson, S. E., Murphy, D. C., Krzeminski, W., Roth, M., & Rieke, M. J. 1998, *AJ*, 116, 2475
- Podsiadlowski, P., Mazzali, P., Lesaffre, P., Han, Z., & Förster, F. 2008, *NewAR*, 52, 381
- Phillips, M. M. 1993, *ApJL*, 413, L105
- Phillips, M. M., Lira, P., Suntzeff, N. B., et al. 1999, *AJ*, 118, 1766
- Phillips, M. M. 2005, 1604-2004: Supernovae as Cosmological Lighthouses, 342, 211
- Phillips, M. M., Simon, J. D., Morrell, N., et al. 2013, *ApJ*, 779, 38
- Prieto, J. L., Rest, A., & Suntzeff, N. B. 2006, *ApJ*, 647, 501
- Perlmutter, S., & Riess, A. 1999, *COSMO-98*, 478, 129
- Riess, A. G., Press, W. H., & Kirshner, R. P. 1996, *ApJ*, 473, 88
- Riess, A. G., Filippenko, A. V., Challis, P., et al. 1998, *AJ*, 116, 1009
- Röpke, F. K., Kromer, M., Seitenzahl, I. R., et al. 2012, *ApJL*, 750, L19
- Schlaflly, E. F., & Finkbeiner, D. P. 2011, *ApJ*, 737, 103
- Schlegel, D. J., Finkbeiner, D. P., & Davis, M. 1998, *ApJ*, 500, 525
- Shappee, B. J. & Thompson, T. A. 2013, *ApJ*, 766, 64.
- Sternberg, A., Gal-Yam, A., Simon, J. D., et al. 2014, *MNRAS*, 443, 1849
- Stritzinger, M. D., Phillips, M. M., Boldt, L. N., et al. 2011, *AJ*, 142, 156
- van den Heuvel, E. P. J., Bhattacharya, D., Nomoto, K., & Rappaport, S. A. 1992, *A&A*, 262, 97
- VanderPlas, J., Fouesneau, M. & Taylor, J. 2014, *Astrophysics Source Code Library*, ascl:1407.018.
- Webbink, R. F. 1984, *ApJ*, 277, 355
- Wood-Vasey, W. M., Friedman, A. S., Bloom, J. S., et al. 2008, *ApJ*, 689, 377-390
- Woosley, S. E., & Weaver, T. A. 1986, *IAU Colloq. 89: Radiation Hydrodynamics in Stars and Compact Objects*, 255, 91
- Yoon, S.-C., & Langer, N. 2003, *A&A*, 412, L53